Redox Biology 37 (2020) 101730

Contents lists available at ScienceDirect

Redox Biology

journal homepage: www.elsevier.com/locate/redox

Research Paper

Rapid, redox-mediated mechanical susceptibility of the cortical microtubule lattice in skeletal muscle

D'anna M. Nelson [a], Elizabeth K. Fasbender [a,b], Margurite C. Jakubiak [a,b], Angus Lindsay [a,c], Dawn A. Lowe [c], James M. Ervasti [a,*]

[a] Department of Biochemistry, Molecular Biology and Biophysics, University of Minnesota, Minneapolis, MN, USA
[b] College of Biological Sciences, University of Minnesota, Minneapolis, MN, USA
[c] Department of Rehabilitation Medicine, University of Minnesota, Minneapolis, MN, USA

ARTICLE INFO

Keywords:
Micro-dystrophin
mdx
NADPH oxidase
Microtubules
Cytoplasmic actin
Duchenne muscular dystrophy
Skeletal muscle
NOX2
nNOS

ABSTRACT

The highly ordered cortical microtubule lattice of skeletal muscle is disorganized in dystrophin-deficient *mdx* mice. Implicated mechanisms include loss of dystrophin binding, altered α-tubulin posttranslational modification, expression of a β-tubulin involved in regeneration, and reactive oxygen species (ROS). Here we show that the transverse microtubules in *mdx* muscle expressing miniaturized dystrophins are rapidly lost after eccentric contraction. Analysis of *mdx* lines expressing different dystrophin constructs demonstrate that spectrin-like repeats R4-15 and R20-23 were required for mechanically stable microtubules. Microtubule loss was prevented by the non-specific antioxidant *N*-acetylcysteine while inhibition of NADPH oxidase 2 had only a partial effect, suggesting that ROS from multiple sources mediate the rapid loss of transverse microtubules after eccentric contraction. Finally, ablation of α-dystrobrevin, β- or γ-cytoplasmic actin phenocopied the transverse microtubule instability of miniaturized dystrophins. Our data demonstrate that multiple dystrophin domains, α-dystrobrevin and cytoplasmic actins are necessary for mechanically stable microtubules.

1. Introduction

Skeletal muscle dystrophin links the cortical actin cytoskeleton to the dystrophin glycoprotein complex (DGC) [1]. As a transmembrane complex, the DGC extends beyond the sarcolemma and connects to the extracellular matrix [2] providing sarcolemmal stability [3]. Patients missing dystrophin protein experience severe muscle pathology known as Duchenne muscular dystrophy (DMD) [4] while Becker muscular dystrophy (BMD) is a milder form of dystrophinopathy that generally results from reduced expression of a less functional dystrophin with internal truncations [5].

Dystrophin has also been shown to play a role in organizing cortical microtubules [6,7], which exist in a highly organized grid positioned longitudinal and transverse to the mouse muscle fiber axis [8]. In the *mdx* mouse model of DMD, the absence of dystrophin is accompanied by loss of transverse microtubules leading to a disorganized microtubule lattice [6,7]. *In vitro* binding studies identified a microtubule binding domain within spectrin-like repeats R20-22 of dystrophin [9]. In contrast, the dystrophin homologue utrophin [10] neither binds microtubules *in vitro* nor restores organization *in vivo* when transgenically expressed in the *mdx* mouse [11]. A dystrophin chimera $Dys^{\Delta MTB}$ with R20-24 swapped for the homologous utrophin R18-22 does not bind microtubules *in vitro* as expected, although it does restore microtubule organization when transgenically expressed in *mdx* mice [9]. While it is clear that the absence of dystrophin impacts *in vivo* microtubule organization, it is unknown which dystrophin domains are involved. Microtubule disorganization in *mdx* muscle has also been associated with altered α-tubulin posttranslational modification [12,13], increased expression of the rare β-tubulin tubb6 during muscle regeneration [14], and altered production of reactive oxygen species (ROS) via NADPH oxidase 2 (NOX2) [15]. Several studies have shown that microtubule disorganization correlates with loss of muscle force production following eccentric (lengthening) contractions [9,11,16], which is one of the most robust and reproducible phenotypes of *mdx* mice [17–19]. Susceptibility to eccentric contraction is also linked to tubulin detyrosination [12,13]. Finally, dystrophin is not sufficient for microtubule organization as loss of the DGC member β-sarcoglycan with retention of dystrophin [9], or loss of neuronal nitric oxide synthase

* Corresponding author. 6 Jackson Hall, 321 Church Street SE, Minneapolis, MN, 55455, USA.
E-mail address: jervasti@umn.edu (J.M. Ervasti).

https://doi.org/10.1016/j.redox.2020.101730
Received 13 July 2020; Received in revised form 12 September 2020; Accepted 12 September 2020
Available online 18 September 2020

(nNOS) [20] also results in microtubule disorganization.

Micro-dystrophins are internally truncated constructs designed to maintain essential dystrophin functions and still fit within adeno-associated virus (AAV) for DMD gene therapy [21]. Micro-dystrophins typically retain the *N*-terminal actin binding domain 1 (ABD1) and the cysteine-rich region that binds to β-dystroglycan in the DGC [22,23]. Micro-dystrophin deletions are targeted to the central rod domain and generally remove nineteen or twenty of the spectrin-like repeats as well as one or two hinges. Micro-dystrophins are also generally deleted for the *C*-terminal 420 residues. Mini-dystrophins are based on the truncated dystrophins expressed in BMD [24,25]. Previous work has shown that micro-dystrophin constructs (lacking R4-23 or R4-15 and R20-23) improve microtubule organization in *mdx* skeletal muscle [7,16]. However, quantitative image analysis demonstrates that micro-dystrophin constructs are less effective than mini-dystrophins in restoring the microtubule lattice organization to wildtype levels [16]. While mini-dystrophins differ from micro-dystrophins by retaining R20-23 that binds microtubules *in vitro* [9], microtubule organization is also fully restored by the dystrophin-utrophin chimera $Dys^{\Delta MTB}$-*mdx* that functionally lacks R20-24 [9]. Thus, previous studies suggest that micro-dystrophins lack a domain required for complete rescue of microtubule organization.

Here we utilized eccentric contractions and quantitative image analysis to investigate the effects of mechanical stress on the microtubule lattice in *mdx* muscle expressing various mini- and micro-dystrophin constructs. Because dystrophin ABD1 is common to all mini- and micro-dystrophins that at least partially rescue microtubule organization in *mdx* skeletal muscle [16], we also investigated microtubule organization before and after eccentric contraction in muscle-specific β-cytoplasmic actin knockout and γ-cytoplasmic actin knockout mice and in transgenic *mdx* mice expressing full length dystrophin with the L172H mutation in ABD1 [26] associated with BMD [27]. We show that *mdx* muscle expressing mini-dystrophins exhibited partial, but significant loss of transverse microtubules immediately following eccentric contraction while *mdx* muscle expressing micro-dystrophins lost all transverse microtubules. We also show that pre-treatment of *mdx* mice expressing a mini- or micro-dystrophin with the antioxidant *N*-acetylcysteine (NAC) completely prevented loss of transverse microtubules after eccentric contraction. More targeted inhibition of NOX2 effected only partial protection of transverse microtubules from eccentric contraction, while three *mdx* lines that protect against eccentric contraction-induced force loss through different perturbations of ROS [28] failed to restore basal microtubule lattice organization. Muscle ablated for β-, or γ-cytoplasmic actin, the DGC component α-dystrobrevin, or transgenic *mdx* muscle expressing the L172H mutant dystrophin all displayed organized microtubules not different from WT, but with loss of transverse microtubules after eccentric contraction. Our study demonstrates the interplay between multiple components of the dystrophin-glycoprotein complex and cytoplasmic actins is necessary for a mechanically stable cortical microtubule lattice.

2. Materials and methods

2.1. Mice

All mice used in this study were adult males (3–5 months of age). Animals were cared for in accordance with, and all experimental protocols were approved by, the University of Minnesota Institutional Animal Care and Use Committee standards. All National Institutes of Health laboratory animal ethical regulations were followed in these studies. C57BL/10 (wildtype) and *mdx* mice were obtained from The Jackson Laboratory. Transgenic dystrophin lines were previously generated: $Dys^{\Delta H2\text{-}R15}$-*mdx* [25], $Dys^{\Delta H2\text{-}R19/\Delta CT}$-*mdx* [24], $Dys^{\Delta R4\text{-}23/\Delta CT}$-*mdx* [29], $Dys^{\Delta R2\text{-}15/\Delta R18\text{-}23/\Delta CT}$-*mdx* [29], Dp116-*mdx* [30] and flμDys (Jeffrey Chamberlain Lab). All transgenic dystrophin lines are skeletal muscle specific via the human skeletal actin promoter (HSA) and were backcrossed onto the *mdx* (C57BL/10ScSn-Dmd^{mdx}/J) mouse strain from The Jackson Laboratory (Bar Harbor, ME). ActB-msCT, Actg1-msCT, ActB-msKO and Actg1-msKO have been previously generated via loxP flanking sites with the knockout mice expressing HSA-Cre [31,32]. *Mdx*/PrxII-TG, *mdx*/$mb^{-/-}$ were previously generated [28] as were the *mdx*/Actg1-TG [33] and $Adbn^{-/-}$ [34]. The genotypes of mini- and micro-dystrophin transgenic mice were verified via amplification of the HSA promoter followed by protein confirmation based upon expected molecular weights and antibody reactivities (S1 Fig).

2.2. In vivo muscle physiology

For all physiology assessments, mice were anesthetized with isoflurane and the lower left hind leg depilated and positioned with the foot perpendicular to the tibia (defined as 0°). Isometric torque generation of the anterior crural muscles (tibialis anterior, extensor digitorum longus, extensor hallucis longus) was elicited by percutaneous stimulation of the peroneal branch of the sciatic nerve (equipment previously described [35]). Voltage was optimized until peak isometric tetanic torque was achieved. Stimulation frequency (typically ~150 Hz) was selected to elicit peak isometric torque as identified during torque-frequency assessment. Train duration during torque optimization was 150 ms. Eccentric Contractions: One set of 70 eccentric contractions was performed interspersed by 10 s. For each eccentric contraction, the foot was passively rotated from 0° to 19° dorsiflexion followed by stimulation during 38° of plantarflexion at 2000°/s. Each eccentric contraction consisted of 100 ms isometric contraction followed by a 20 ms eccentric contraction during plantarflexion. Isometric Contractions: One set of 70 isometric contractions were carried out using the above eccentric contraction protocol in the absence of any rotation about the ankle. Passive Lengthening: One set of 70 passive lengthening cycles were carried out using the above eccentric contraction protocol in the absence of electrical stimulation (no muscle contraction). *N*-acetylcysteine (NAC) Treatment: Mice were given a single intraperitoneal injection of 150 mg/kg NAC (Sigma-Aldrich, St. Louis, MO) dissolved in PBS and adjusted to neutral pH. NAC was administered 1 h before electrode insertion for stimulation of the anterior crural muscles. GSK2795039 Treatment: Mice were given a single intraperitoneal injection of 100 mg/kg GSK2795039 (GlpBio Technology, Montclair, CA) dissolved in 20% DMSO/20% Tween 80/60% polyethylene glycol 200, administered 1 h before subcutaneous electrode insertion. GSK2795039 solution was prepared at 3 mg/100 μL, allowing each mouse to receive less than 150 μL total volume. Recovery Timeline: Mice utilized for the microtubule recovery timeline performed the eccentric contraction protocol and were allowed to recover for 5 or 10 days before euthanasia via anesthetized cervical dislocation for muscle collection. All other mice (Eccentric/Isometric/Passive Lengthening/N-acetylcysteine/GSK2795039) had muscles harvested immediately following completion of the physiology assay (~30 min after first eccentric contraction, ~10 min after last eccentric contraction). In each physiological assay, the left leg performed the protocol while the right leg served as a contralateral control.

2.3. Muscle fiber imaging

EDLs used in Fig. 1 were harvested from perfusion fixed mice as previously described [16]. Perfusion was performed immediately following eccentric contraction. Subsequent experiments utilized the below described collagenase and fix protocol. Characterization of both protocols on multiple genotypes did not reveal any differences in the results. Lower hind limbs were harvested and digested in 0.2% type I collagenase (Sigma-Aldrich, St. Louis, MO) in DMEM (Gibco) for 70 min at 37 °C and 5% CO_2 to allow penetration of fixative to interior fibers. Limbs were fixed in 4% paraformaldehyde (Thermo Fisher, Waltham,

MA) in PBS with the ankle plantarflexed approximately 40° for 70 min at room temperature. The EDL muscle was dissected and then fibers were manually separated and blocked with 5% goat serum/0.1% Triton X-100 in PBS for 60 min at room temperature. Fibers were incubated with 1:200 *anti*-α-tubulin (DM1A; Sigma Aldrich) overnight at room temperature with rotation. Secondary staining with goat *anti*-mouse Alexa Fluor 568 at 1:250 (Invitrogen) for 2 h at room temperature was used for visualization. At least ~150 fibers were stained per EDL. Fibers were mounted on slides using Prolong Gold antifade reagent with DAPI (Cell Signaling Technology) to visualize nuclei. Fibers were imaged at 60× on the Olympus FluoView FV1000. All stained fibers were considered to determine representative fibers for imaging. The entire length of fibers was considered when determining a region for image capture. ImageJ sum slices projection was used to combine Z-stacks of one to three sarcolemmal images (total depth of 0.4–1.2 μm). Brightness and contrast were adjusted using ImageJ equivalently across experimental and control images. Images were representative of $N \geq 3$ mice per genotype or physiology assay and $n \geq 10$ fibers per mouse.

2.4. Quantitative microtubule lattice analysis

Microtubule directionality was determined using the TeDT program [36] and quantified in 4° increments from 0 to 176°. All images were analyzed such that longitudinal microtubules were at 0 and 180° and transverse microtubules were at 90°. Percent transverse microtubule loss reported in the text was an average of the percent loss at 88° and 92°. Microtubules near nuclei were not included in the analysis. Microtubule lattice directionality for each genotype/physiology assay consisted of minimally $N \geq 3$ mice per genotype or assay and $n \geq 10$ fibers per mouse. Microtubule directionality proportions were normalized to extend between 0 and 1 (Relative H_D). TeDT values for each fiber analyzed were utilized to create an average TeDT plot for each animal. The average TeDT values for each animal within a genotype or assay were used to create an overall TeDT plot for that genotype or assay.

2.5. Microtubule enrichment

Gastrocnemius muscles were mechanically disrupted with mortar and pestle in liquid nitrogen. Ground tissue was lysed with 1% Triton X-100 in microtubule buffer (50 mM HEPES, 50 mM KCl, 1 mM $MgCl_2$, 1 mM EGTA, pH 7.5 with KOH) with protease inhibitors (100 μM Aprotinin, 0.79 mg/mL Benzamide, 10 nM E−64, 10 μM Leupeptin, 0.1 mg/mL Pepstatin, 1 mM phenylmethylsulfonyl fluoride; Sigma-Aldrich). Lysate was incubated for 40 min and centrifuged at 14,000 rpm for 30 min, both at 4 °C. Supernatant was incubated with 4 mM GTP (Cytoskeleton, Denver, CO) and 1 mM DTT (MilliporeSigma, St. Louis, MO) for 40 min at 37 °C. Twenty μM Taxol (Cytoskeleton, Denver, CO) was added for an additional 60 min. Supernatant was layered on cushion buffer of 40% glycerol in microtubule buffer at 1:1 ratio and centrifuged at 50,000 rpm for 30 min at 37 °C. Pellets were rinsed with acetone.

2.6. DGC enrichment

Gastrocnemius muscles were mechanically disrupted with mortar and pestle in liquid nitrogen. Ground tissue was lysed with 1% Triton X-100 in 1xPBS with protease inhibitors (same inhibitors as microtubule enrichment). Samples were rotated and then centrifuged at 14,000 rpm, each for 30 min at 4 °C. The cleared lysate was added to wheat germ agglutinin beads (Vector Laboratories, Burlingame, CA) and rotated at 4 °C overnight. The beads and lysate mixture was then centrifuged at 5000 rpm for 3 min at 4 °C to collect beads. After centrifugation, the void liquid was removed and the beads washed 3× with PBS. One percent sodium dodecyl sulfate in 1xPBS was added to the beads prior to boiling for 5 min. The beads were then pelleted and the supernatant collected. Proteins were precipitated with acetone as well as the pellet being rinsed with acetone.

2.7. Tandem mass tags (TMT) proteomics

Proteomics was performed with the guidance of the Center for Mass Spectrometry and Proteomics at the University of Minnesota. Experimental Design: From each mouse, one gastrocnemius was used for microtubule enrichment and the other for DGC enrichment. Two paired 10plex TMT experiments were used to compare sixteen unique DGC (or microtubule) enrichments (four genotypes, each with $n = 4$) plus four pooled samples to allow comparison across the two individual 10plex experiments for microtubules or DGC. Each experimental line ($Dys^{\Delta H2\text{-}R15}$-*mdx*, $Dys^{\Delta MTB}$-*mdx*, $Dys^{\Delta R4\text{-}23/\Delta CT}$-*mdx*) was compared to the control line $Dys^{\Delta 71\text{-}78}$-*mdx* to allow identification of proteins for which there was a significant log 2 fold change in expression in experimental compared to control. Proteins of interest were those significantly different in all 3 experimental lines compared to $Dys^{\Delta 71\text{-}78}$-*mdx* (R4-15 and R20-23 connection), those altered similarly in $Dys^{\Delta H2\text{-}R15}$-*mdx* and $Dys^{\Delta R4\text{-}23/\Delta CT}$-*mdx* but not changed in $Dys^{\Delta MTB}$-*mdx* compared to $Dys^{\Delta 71\text{-}78}$-*mdx* (R4-15 connection), and those altered similarly in $Dys^{\Delta MTB}$-*mdx* and $Dys^{\Delta R4\text{-}23/\Delta CT}$-*mdx* but not changed in $Dys^{\Delta H2\text{-}R15}$-*mdx* compared to $Dys^{\Delta 71\text{-}78}$-*mdx* (R20-23 connection). Protein Solubilization: All samples for the microtubule (MT) set and DGC set were prepared as follows: Pellets were resuspended with a 100 μL of solubilization buffer [7 M urea, 2 M thiourea, 0.4 M triethylammonium bicarbonate (TEAB) pH 8.5, 20% acetonitrile and 4 mM tris(2-carboxyethyl)phosphine (TCEP)]. The samples were vortexed briefly, then sonicated. Each sample was transferred to a PCT tube for further disruption with a Barocycler NEP2320 (Pressure Biosciences, Inc., South Easton, MA). 200 mM methyl methanethiosulfonate (MMTS) was added to a final concentration of 8 mM MMTS. Aliquots of each sample were taken for protein concentration determination by Bradford assay. In-Solution Proteolytic Digestion and TMT10plex™ Isobaric Labeling: Thirty μg samples (individual and pooled—pooled consisted of 1/16 of each DGC or MT sample) were brought to the same volume with protein solubilization buffer plus 8 mM MMTS. All samples (individual and pooled) were diluted five-fold with ultra-pure water and trypsin (Promega, Madison, WI) was added in a 1:40 ratio of trypsin to total protein for overnight digestion. After being dried, samples were cleaned with a 1 mL Sep-Pak C18 SPE cartridge (Waters Corporation, Milford, MA). Each sample set was labeled with a corresponding TMT10plex™ Isobaric Label Reagent Set, 1 × 0.8 mg (Thermo Scientific, Watham, MA) per manufacturer's protocol with the following exception. Each 10plex 0.8 mg reagent vial was brought up in 82 μL of acetonitrile, vortexed, spun down and 41 μL of 10plex reagent was added to its respective sample. After labeling, all the samples within each TMT 10plex experiment were multiplexed together into a new 1.5 mL microfuge tube and vacuum dried. The multiplexed TMT samples were cleaned with a 3 cc Oasis MCX solid phase extraction cartridge (Waters Corporation, Milford, MA) and the eluate was dried *in vacuo*. 1st Dimension Peptide Liquid Chromatography Fractionation: The TMT10plex™ Isobaric labeled samples were fractionated offline by high pH C18 reversed-phase (RP) chromatography. The flow rate was 200 μL/min with fractions collected every 2 min and UV absorbances were monitored at 215 nm and 280 nm. Peptide containing fractions were divided into two equal numbered groups, "early" and "late". Equal milliabsorbance units (mAU) of the first "early" fraction was concatenated with the first "late" fraction, and so on. Acquisition of nano-liquid chromatography tandem mass spectrometry: LC-MS data was acquired for each concatenated fraction using an Easy-nLC 1000 HPLC (Thermo Scientific Inc., Waltham, MA) in tandem with a Thermo Fisher Orbitrap Fusion (Thermo Scientific Inc., Waltham, MA). The column was mounted in a nanospray source directly in line with an Orbitrap Fusion mass spectrometer (Thermo Scientific). The orbital trap was set to acquire survey mass spectra (380–1580 *m/z*) with a resolution of 60,000 at 100 *m/z* with automatic gain control (AGC) 1.0E6, 250-ms min injection time and lock mass at 445.1200 *m/z* (polysiloxane). The 12 most intense ions (2–7 charged state) from the full scan were selected for fragmentation by higher-energy collisional dissociation with

normalized collision energy 35%, and detector settings of 60 k resolution, AGC 5E4 ions, 250 ms maximum injection time and FT first mass mode fixed at 110 *m/z*. Dynamic exclusion was set to 40 s with a 10 ppm high and low mass tolerance. Database searching for protein detection: The tandem mass spectra were analyzed using Sequest (XCorr Only) in Proteome Discoverer 2.2.0.388 (Thermo Fisher Scientific, Waltham, MA). We used the NCBI Reference Sequence mouse protein sequence database (taxon ID 10088) from Aug 22, 2018 merged with the common lab contaminant protein database from https://www.thegpm.org/crap/, with a total of 185,018 entries, for the database searching. The Sequest search parameters included: trypsin enzyme, fragment ion mass tolerance of 0.1 Da, precursor ion tolerance 50 ppm, *S*-methylthiocysteine as a fixed modification; pyroglutamic acid from glutamine, deamidation of asparagine, oxidation of methionine, *N*-terminal protein acetylation and TMT 10plex for lysine and peptide *N*-termini as variable modifications. Relative protein quantification: Scaffold Q+ (v4.9, Proteome Software Inc., Portland, OR) was used for relative quantification of proteins. Peptide identifications were accepted if they could be established at greater than 89.0% probability to achieve an FDR less than 1.0% by the Scaffold Local FDR algorithm. Protein identifications were accepted if they could be established at greater than 5.0% probability to achieve an FDR less than 1.0% and contained at least 2 identified peptides. Protein probabilities were assigned by the Protein Prophet algorithm. Proteins that contained similar peptides and could not be differentiated based on MS/MS analysis alone were grouped to satisfy the principles of parsimony. Proteins sharing significant peptide evidence were grouped into clusters. Channels were corrected for incomplete isotope incorporation in all samples according to the algorithm described in i-Tracker. Normalization was performed iteratively (across samples and spectra) on intensities. Medians were used for averaging. Spectra data were log-transformed, pruned of those matched to multiple proteins, and weighted by an adaptive intensity weighting algorithm. Of 46,922 spectra in the experiment at the given thresholds, 34,528 (74%) were included in quantitation. Results from the two 10-plex DGC or microtubule experiments were merged into a single report with duplicate 'pooled-control' reference channels assigned for normalization across experiments. Differentially expressed proteins were determined by applying Permutation Test with unadjusted significance level $p < 0.05$ corrected by the Benjamini-Hochberg method.

2.8. Western blot analysis

Gastrocnemius (Fig. 2B) or EDL (Fig. 2C-E) muscles were mechanically disrupted with mortar and pestle in liquid nitrogen. Ground tissue was lysed with 1% sodium dodecyl sulfate in 1xPBS with protease inhibitors (same inhibitors as microtubule enrichment). Protein lysate was clarified by centrifugation and concentration measured by A_{280} absorbance. Fifty μg of total protein was loaded on a 10% polyacrylamide gel for 1.25 h at 150 V. Protein was transferred to polyvinylidene fluoride membrane (Millipore Sigma) at 0.8 A for 1 h. Membranes were blocked in 5% non-fat milk in PBS for 1 h. Primary antibodies including 1:10,000 *anti*-DeTyr-tubulin (gift from Dr. Gregg Gundersen [37]), 1:1000 *anti*--α-tubulin (DM1A, Sigma Aldrich), 1:500 *anti*-tubb6 (own generation), and 1:10,000 *anti*-GAPDH (G8795 & G9545, Sigma Aldrich) were incubated overnight at 4 °C. Secondary antibodies, DyLight 680 and 800 (1:10,000, Cell Signaling), were incubated for 1 h at room temperature. Membranes were imaged and band density quantified with a Licor Odyssey Infrared Imaging System and accompanying software. Western blots (Fig. 2) were representative of $n = 4$ for gastrocnemius and $n = 5$ for EDL muscles.

2.9. Statistics

Two-way repeated measures ANOVAs were utilized to compare contralateral to experimental condition (eccentric, isometric, lengthening) within each genotype for Figs. 1, 3, 5 and 6, S2, S3 and S4. Factors were microtubule angle and EDL muscles. EDL from the same mouse (contralateral and experimental) was the repeated factor. Ordinary two-way ANOVAs were utilized to compare contralateral organization in actin CT vs KO in Fig. 5, as well as to compare *mdx*/Actg1-TG, *mdx*/PrxII-TG and *mdx*/$mb^{-/-}$ to their respective *mdx* cohorts in Fig. 4. Any ANOVA with a significant interaction was followed by Bonferroni multiple comparison tests to compare EDLs at each angle. ANOVA interaction and Bonferroni results are reported in the figure legends. Asterisks denoting significance in Figs. 1, 3, 5 and 6, S2, S3, and S4 are based on Bonferroni multiple comparison significance values (* = $p < 0.05$, ** = $p < 0.01$, *** = $p < 0.001$).

Statistical analysis for proteomic comparisons shown in S5 Fig used permutation tests with Benjamini-Hochberg correction for statistical significance. Fig. 2B utilized one-way ANOVA with Dunnett's multiple comparison. Fig. 2C–E utilized two-tailed paired t-tests. All statistical analyses were calculated using GraphPad Prism v8 except for S5 Fig and S1–S8 Data which utilized Scaffold v4. All data are presented as mean ± SEM.

2.10. Data availability

All shareable materials will be released upon completion of a materials transfer agreement. The proteomics dataset generated during the current study has been deposited to the Proteome Xchange Consortium with the dataset identified PXD021088.

3. Results

3.1. Eccentric contraction causes rapid loss of transverse microtubules in mdx mice expressing miniaturized dystrophins

Because microtubule disorganization correlates with increased sensitivity to eccentric contraction [9,11,16], we asked if eccentric contractions influence the microtubule lattice through analysis of different miniaturized dystrophin transgenes expressed in *mdx* skeletal muscle (Fig. 1A and S2 Fig). In wildtype C57BL/10 extensor digitorum longus (EDL) muscle, *in vivo* eccentric contractions did not cause detectable microtubule alterations (Fig. 1B and C). However, in two lines expressing mini-dystrophins ($Dys^{\Delta H2\text{-}R15}$-*mdx* and $Dys^{\Delta H2\text{-}R19/\Delta CT}$-*mdx*) lacking R4-15, we measured significant ~50% loss of transverse microtubules following eccentric contraction (Fig. 1B and C). $Dys^{\Delta MTB}$-*mdx* lacking dystrophin R20-24 exhibited a similar degree of transverse microtubule loss (Fig. 1B and C). When both R4-15 and R20-23 were absent as in micro-dystrophins $Dys^{\Delta R4\text{-}23/\Delta CT}$-*mdx* and $Dys^{\Delta R2\text{-}15/\Delta R18\text{-}23/\Delta CT}$-*mdx*, all transverse microtubules were lost following eccentric contraction (Fig. 1B, D). As a negative control, eccentric contractions caused no change in the microtubule lattice of $Dys^{\Delta 71\text{-}78}$-*mdx* muscle (Fig. 1B, D).

Eccentric contractions involve both active force production combined with muscle lengthening, so we investigated which component(s) were necessary for transverse microtubule loss in *mdx* muscles expressing mini- or micro-dystrophin. Neither tetanic isometric contractions (S3 Fig A, C), nor passive lengthening (S3 Fig B, D) had an effect on the microtubule lattice in $Dys^{\Delta H2\text{-}R15}$-*mdx* or $Dys^{\Delta R4\text{-}23/\Delta CT}$-*mdx* muscle. Because the rapid loss of transverse microtubules after eccentric contraction suggests altered microtubule dynamics, we investigated the rate of transverse microtubule recovery after eccentric contraction-induced loss. The microtubule lattice of $Dys^{\Delta H2\text{-}R15}$-*mdx* or $Dys^{\Delta R4\text{-}23/\Delta CT}$-*mdx* exhibited significant transverse microtubule loss five days after eccentric contraction (S4 Fig A, C), while transverse microtubules did not differ from corresponding contralateral muscles 10 days after eccentric contraction (S4 Fig B, D). Thus, transverse microtubules are lost in *mdx* muscle expressing truncated dystrophins within minutes of eccentric contraction but recover much more slowly over a period of days.

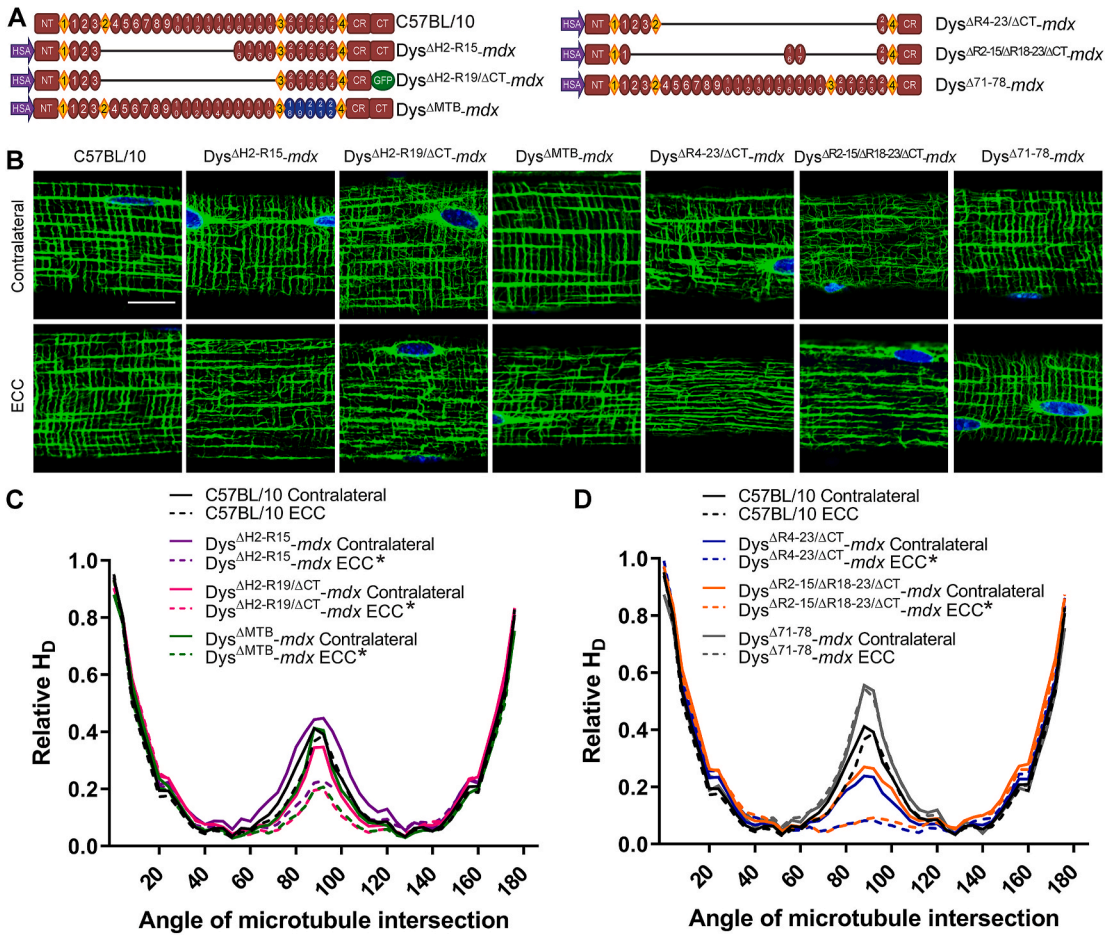

Fig. 1. The absence of dystrophin spectrin-like repeats R4-15 and R20–23 resulted in transverse microtubule susceptibility to eccentric contraction (ECC). A) Schematic of wildtype dystrophin and the skeletal muscle specific transgenic dystrophin constructs expressed in *mdx* that were utilized in this study. HSA, human skeletal α-actin promoter; NT, *N*-terminus; diamonds represent hinge regions; ovals represent spectrin-like repeats (maroon are dystrophin, blue are utrophin); CR, cysteine-rich domain; CT, C-terminus. B) Cortical microtubule lattice of contralateral or eccentrically contracted (ECC) EDL fibers. Nuclei are blue, tubulin in green, scale bar is 20 μm, 60× magnification. Images are representative of those obtained for n ≥ 10 fibers from N = 3 mice (Dys$^{\Delta H2\text{-}R15}$-*mdx*, Dys$^{\Delta 71\text{-}78}$-*mdx*), N = 4 mice (Dys$^{\Delta R4\text{-}23/\Delta CT}$-*mdx*), N = 5 mice (C57BL/10, Dys$^{\Delta H2\text{-}R19/\Delta CT}$-*mdx*, Dys$^{\Delta R2\text{-}15/\Delta R18\text{-}23/\Delta CT}$-*mdx*), or N = 6 mice (Dys$^{\Delta MTB}$-*mdx*). C) C57BL/10 microtubule directionality did not change upon eccentric contraction. Dys$^{\Delta H2\text{-}R15}$-*mdx*, Dys$^{\Delta H2\text{-}R19/\Delta CT}$-*mdx* and Dys$^{\Delta MTB}$-*mdx* exhibited ~50% loss in the proportion of transverse microtubules upon ECC. D) Micro-dystrophins Dys$^{\Delta R4\text{-}23/\Delta CT}$-*mdx* and Dys$^{\Delta R2\text{-}15/\Delta R18\text{-}23/\Delta CT}$-*mdx* were highly susceptible to transverse microtubule loss after eccentric contraction. The microtubule lattice of Dys$^{\Delta 71\text{-}78}$-*mdx* was not affected by eccentric contraction. Two-way repeated measures ANOVA was used to compare contralateral to ECC within each genotype. Significant interactions ($p < 0.0001$) were found for Dys$^{\Delta H2\text{-}R15}$-*mdx*, Dys$^{\Delta H2\text{-}R19/\Delta CT}$-*mdx*, Dys$^{\Delta MTB}$-*mdx*, Dys$^{\Delta R4\text{-}23/\Delta CT}$-*mdx*, Dys$^{\Delta R2\text{-}15/\Delta R18\text{-}23/\Delta CT}$-*mdx*. Bonferroni multiple comparison tests revealed significant (*$p < 0.05$) differences between contralateral and ECC at the following angles: 68°–100° (Dys$^{\Delta H2\text{-}R15}$-*mdx*), 80°–100° (Dys$^{\Delta H2\text{-}R19/\Delta CT}$-*mdx*), 76°–104° (Dys$^{\Delta MTB}$-*mdx*), 76°–96° (Dys$^{\Delta R4\text{-}23/\Delta CT}$-*mdx*), 76°–100° (Dys$^{\Delta R2\text{-}15/\Delta R18\text{-}23/\Delta CT}$-*mdx*). In analyses where the interaction was not significant, the main effect of the EDL was p = 0.0001 (C57BL/10) and p = 0.031 (Dys$^{\Delta 71\text{-}78}$-*mdx*). Error bars were omitted to not obstruct the plots.

3.2. Proteomic changes underlying transverse microtubule instability

Dystrophin R4-15 and R20-23 both appear to have roles in basal microtubule organization and microtubule stabilization during eccentric contraction; however, it is not clear whether either domain acts through a direct binding interaction with microtubules [9]. Therefore, we sought to identify proteins that may bridge an interaction between dystrophin R4-15/R20-23 and microtubules using a paired, 10plex tandem mass tags proteomic screen that allowed comparison of four mouse lines (Dys$^{\Delta 71\text{-}78}$-*mdx*, Dys$^{\Delta H2\text{-}R15}$-*mdx*, Dys$^{\Delta MTB}$-*mdx*, Dys$^{\Delta R4\text{-}23/\Delta CT}$-*mdx*). The experimental design permitted comparison between lines expressing dystrophin constructs lacking one region (Dys$^{\Delta H2\text{-}R15}$-*mdx*, Dys$^{\Delta MTB}$-*mdx*), or both regions (Dys$^{\Delta R4\text{-}23/\Delta CT}$-*mdx*) of interest. All three lines with domain deletion were compared to Dys$^{\Delta 71\text{-}78}$-*mdx*, which had both domains of interest and controlled for the *mdx* background. Proteomic screens were performed on both DGC and microtubule enriched fractions from each line, and data were analyzed to identify proteins that may associate with R4-15, R20-23, or both regions (S5 Fig, S1–S8 Data). Twelve proteomic hits were selected for further validation including five that showed domain specific alterations and seven that were influenced by both domains but also had proposed interplay with either microtubules or dystrophin. Quantitative Western blot analysis of the twelve hits yielded no proteins that could provide a mechanism by which R4-15 or R20-23 regulated stable microtubule organization (S9 Data).

3.3. Rapid changes in posttranslational modification support altered microtubule dynamics

In addition to microtubule disorganization, *mdx* muscle presents with alterations in expression of a specific tubulin isoform and post-translational modifications [6,9,12–15]. Because increased expression of the rare beta tubulin isoform tubb6 is associated with altered microtubule organization and muscle regeneration in the *mdx* mouse [14], we measured tubb6 levels in Dys$^{\Delta H2\text{-}R15}$-*mdx*, Dys$^{\Delta H2\text{-}R19/\Delta CT}$-*mdx*,

Dys$^{\Delta R4\text{-}23/\Delta CT}$-*mdx* and Dys$^{\Delta R2\text{-}15/\Delta R18\text{-}23/\Delta CT}$-*mdx* (constructs shown in Fig. 1A), an additional micro-dystrophin flμDys-*mdx* with flanking loxP sites, and Dp116-*mdx* which expressed a short, neuronal dystrophin isoform [16] (Fig. 2A). All *mdx* muscles expressing mini- or micro-dystrophins had tubb6 levels not different from wildtype, while tubb6 in Dp116-*mdx* (which had disorganized microtubules) [16] and *mdx* trended towards elevated levels compared to wildtype (Fig. 2B). The level of tubb6 also did not change in micro-dystrophin (Dys$^{\Delta R2\text{-}15/\Delta R18\text{-}23/\Delta CT}$-*mdx*) muscle following eccentric contraction (Fig. 2C). These data suggest that neither tubb6 expression nor regeneration [14] impact microtubule organization in *mdx* mice expressing mini- or micro-dystrophin either before or after eccentric contraction. Detyrosinated α-tubulin is a post-polymerization modification that marks stable microtubules [38,39] and is significantly elevated in *mdx* muscle compared to wildtype [9,12,15]. We found that detyrosinated α-tubulin was significantly decreased in micro-dystrophin Dys$^{\Delta R2\text{-}15/\Delta R18\text{-}23/\Delta CT}$-*mdx* muscle following eccentric contraction (Fig. 2D) while total α-tubulin levels were increased (Fig. 2E). Decreased detyrosination is likely associated with microtubule depolymerization. Based on the rapid tissue harvest post eccentric contraction, we hypothesize the increased α-tubulin immunoreactivity is due to either increased tubulin solubility or altered post translational modifications that impact immunoreactivity.

3.4. *Multiple sources of ROS are involved in rapid transverse microtubule loss after eccentric contraction*

ROS have been implicated in mediating rapid eccentric contraction-induced force loss in *mdx* muscle [19,28]. We pretreated *mdx* mice expressing either a mini- or micro-dystrophin with the non-specific antioxidant *N*-acetylcysteine (NAC) and assessed microtubule organization after eccentric contraction. Interestingly, one hour pretreatment with NAC completely prevented transverse microtubule loss in Dys$^{\Delta H2\text{-}R15}$-*mdx* and Dys$^{\Delta R4\text{-}23/\Delta CT}$-*mdx* muscles (Fig. 3A and B). Because NOX2 has been implicated in disrupting basal microtubule organization in *mdx* muscle [15], we investigated the efficacy of the NOX2 inhibitor GSK2795039 [40] to protect transverse microtubules from eccentric contraction in *mdx* muscle expressing truncated dystrophin. One hour pretreatment of Dys$^{\Delta R4\text{-}23/\Delta CT}$-*mdx* mice with GSK2795039 effected a significant, but partial protection of transverse microtubules after eccentric contraction (Fig. 3A, C). Because genetic ablation of NOX2 improves basal microtubule organization in *mdx* muscle [15] and partially protects it from eccentric contraction-induced force loss [28], we analyzed microtubule organization in three additional *mdx* lines that were genetically modified to either reduce or alter the chemical nature of ROS and have highly similar protection from eccentric contraction-induced force loss [28]. However, we found that the microtubule lattice remained disorganized in *mdx* muscles overexpressing γ-cytoplasmic actin (*mdx*/Actg1-TG) (Fig. 4A and B), the antioxidant peroxiredoxin II (*mdx*/PrxII-TG), or after genetic ablation of myoglobin (*mdx*/mb$^{-/-}$) (Fig. 4C and D), suggesting that ROS perturbations that are protective of *mdx* muscle during eccentric contraction do not always correspond to improved microtubule organization. Based on these data, we conclude that multiple sources of ROS must uniquely contribute to rapid eccentric contraction-induced loss of transverse microtubules. We can confirm a role for NOX2 (Fig. 3), but not nNOS

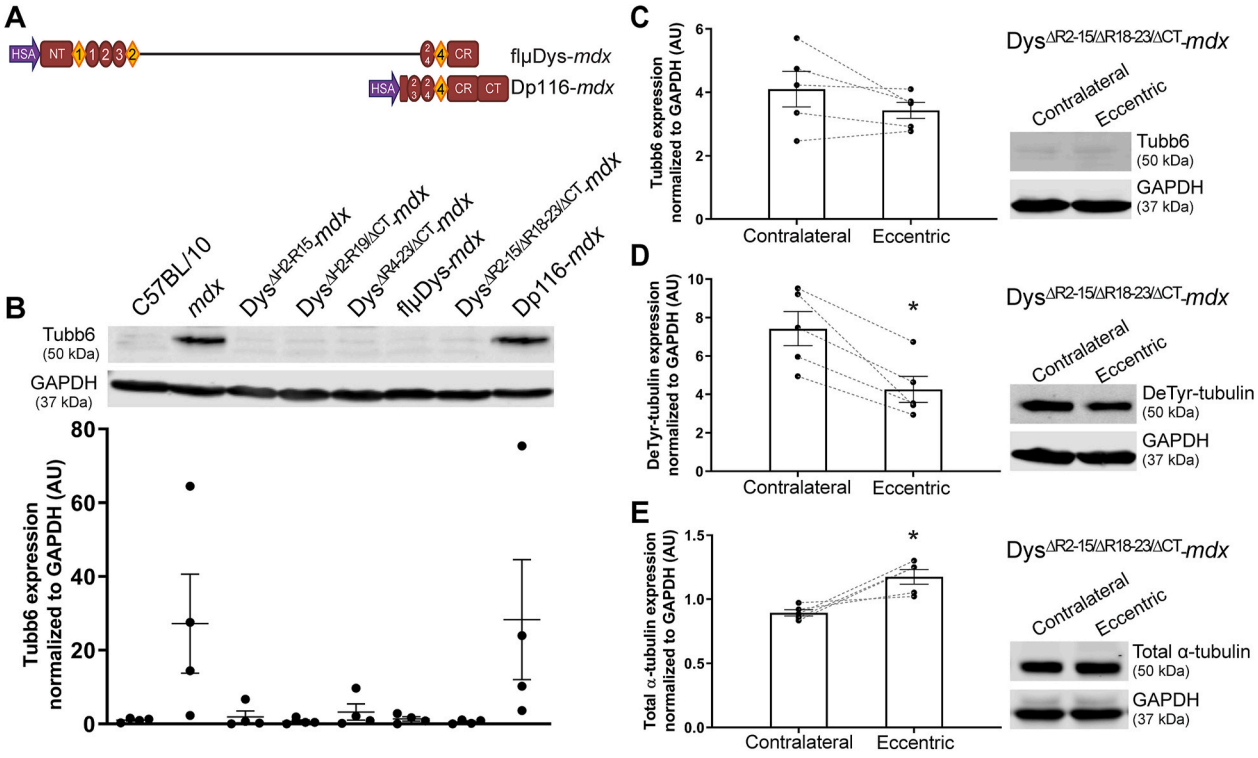

Fig. 2. Tubb6 protein levels were reduced by expression of mini- or micro-dystrophin in *mdx* muscle and did not change after eccentric contractions. A) Two additional dystrophin constructs expressed as skeletal muscle specific transgenes in *mdx* that were examined in Fig. 2B. B) Tubb6 levels trended towards elevated in *mdx* and Dp116-*mdx* muscle. The two mini-dystrophins and three micro-dystrophins all reduced tubb6 to levels not different from wildtype. One-way ANOVA was significant ($p = 0.037$), however Dunnett's multiple comparisons test of each genotype to C57BL/10 failed to identify any significantly different genotype (*mdx* vs C57BL/10, $p = 0.105$; Dp116-*mdx* vs C57BL/10, $p = 0.085$). $N = 4$ per genotype. C) Tubb6 expression was not different in contralateral versus eccentrically contracted micro-dystrophin Dys$^{\Delta R2\text{-}15/\Delta R18\text{-}23/\Delta CT}$-*mdx* muscle. Paired *t*-test ($p = 0.178$), $N = 5$. D) There was a very significant reduction in DeTyr-tubulin levels in eccentrically contracted micro-dystrophin EDLs. Paired *t*-test (*$p = 0.009$), $N = 5$. E) Total α-tubulin levels were slightly elevated in post eccentric contraction micro-dystrophin muscle. Paired *t*-test (*$p = 0.023$), $N = 5$. Matched EDLs from a single animal are connected by dashed lines. Expression levels are normalized to GAPDH and displayed in arbitrary units (AU). All tubulin species are 50 kDa and GAPDH is 37 kDa.

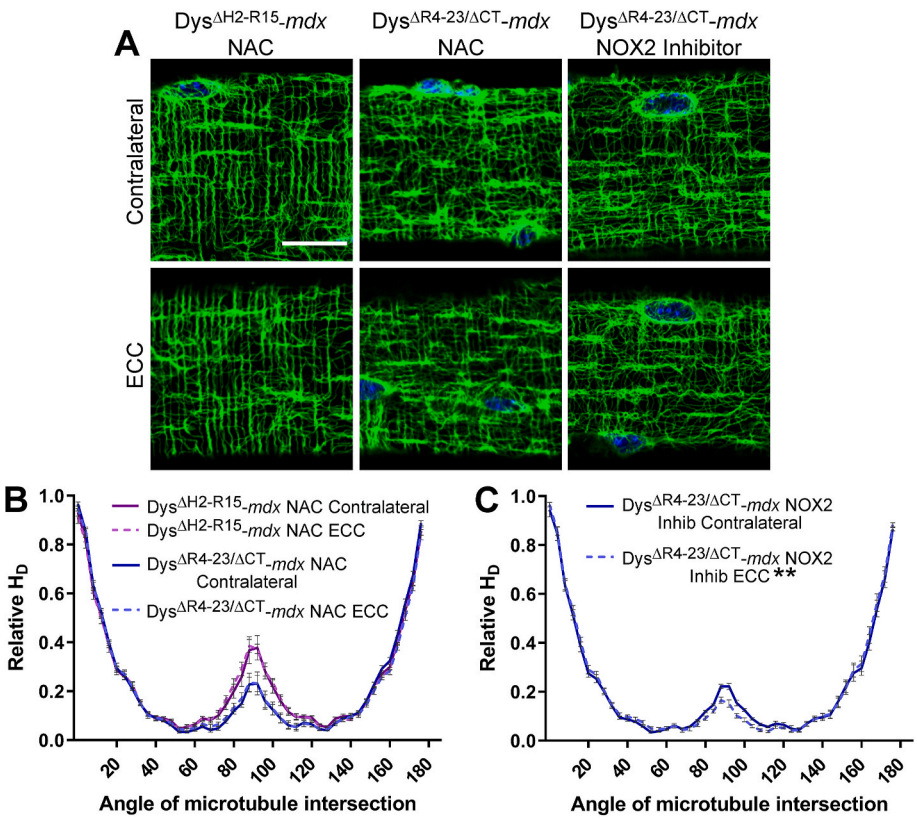

Fig. 3. *N*-acetylcysteine prevented transverse microtubule loss while inhibition of NOX2 showed partial protection of transverse microtubules from eccentric contraction. A) Cortical microtubule lattices from contralateral and eccentrically contracted EDLs that had been pre-treated with NAC (Dys$^{\Delta H2\text{-}R15}$-*mdx* and Dys$^{\Delta R4\text{-}23/\Delta CT}$-*mdx*) or pretreated with GSK2795039 to inhibit NOX2 (Dys$^{\Delta R4\text{-}23/\Delta CT}$-*mdx*). B) NAC prevented loss of transverse microtubules in both mini-dystrophin Dys$^{\Delta H2\text{-}R15}$-*mdx* and micro-dystrophin Dys$^{\Delta R4\text{-}23/\Delta CT}$-*mdx*. C) Inhibition of NOX2 did not completely prevent transverse microtubule loss in Dys$^{\Delta R4\text{-}23/\Delta CT}$-*mdx*. Two-way repeated measures ANOVA did not have a significant interaction in NAC treated Dys$^{\Delta H2\text{-}R15}$-*mdx*. A significant interaction ($p = 0.022$) was present in NAC treated Dys$^{\Delta R4\text{-}23/\Delta CT}$-*mdx*, however Bonferroni multiple comparison tests revealed no significant difference for the transverse microtubule populations (88° and 92° $p > 0.999$). A significant interaction ($p < 0.0001$) also existed for GSK2795039 treated Dys$^{\Delta R4\text{-}23/\Delta CT}$-*mdx*, Bonferroni multiple comparison tests were significant (*$p < 0.01$) at 88°–100°. Nuclei are blue, tubulin in green. Scale bar is 20 μm, 60× magnification. Images are representative of $n \geq 10$ fibers from $N = 5$ (Dys$^{\Delta H2\text{-}R15}$-*mdx*) and $N = 4$ (Dys$^{\Delta R4\text{-}23/\Delta CT}$-*mdx*). In analyses where the interaction was not significant (NAC treated Dys$^{\Delta H2\text{-}R15}$-*mdx*), the main effect of the EDL was also not significant. Error bars are mean ± SEM.

based on identical transverse microtubule mechanical instability in *mdx* mice expressing truncated dystrophins that contain or lack the R16-17 nNOS localization motif (Fig. 1). Therefore, other sources of ROS seem likely to contribute.

3.5. Cytoplasmic actins are required for a mechanically stable microtubule lattice

Because all miniaturized dystrophin constructs that at least partially rescue microtubule lattice organization contain ABD1, and dystrophin interacts with cytoplasmic actins *in vivo* [32,41], we analyzed the cortical microtubule lattice in EDL muscles from muscle-specific β-cytoplasmic actin (ActB-msKO) and γ-cytoplasmic actin (Actg1-msKO) knockout mice. Basal microtubule organization in ActB-msKO and Actg1-msKO muscles were not different from control muscles ActB-msCT and Actg1-msCT (Fig. 5A and B). However, eccentric contractions caused significant loss (30–40%) of transverse microtubules in ActB-msKO (Fig. 5A, C, E) or Actg1-msKO muscles (Fig. 5B, D, F). In parallel, we also assessed how a missense mutation in ABD1 associated with BMD affected cortical microtubule lattice stability. Microtubule organization in transgenic L172H-*mdx* mice has been previously shown to be indistinguishable from wildtype [26]. However, we observed significant 40% loss of transverse microtubules in L172H-*mdx* EDL muscles challenged with eccentric contraction (Fig. 6A and B). Collectively, these data demonstrate the interplay between dystrophin and cytoplasmic actins in supporting a mechanically stable cortical microtubule lattice in skeletal muscle.

3.6. Dystrophin-independent microtubule instability

Genetic ablation of the DGC member β-sarcoglycan results in loss of cortical microtubule organization even in the presence of near normal sarcolemmal dystrophin expression [9]. Therefore, we analyzed the microtubule lattice in mice null for the DGC component α-dystrobrevin (Adbn). The basal microtubule lattice of Adbn$^{-/-}$ muscle was highly organized (Fig. 6C). Once again, however, we measured significant loss of transverse microtubules in Adbn$^{-/-}$ muscles after eccentric contraction (Fig. 6B). In summary, we have demonstrated a common mechanical instability in the cortical microtubule lattice of skeletal muscles lacking subdomains of dystrophin, molecular binding partners of dystrophin, and subunits of the DGC.

4. Discussion

Skeletal muscle microtubules have roles in muscle differentiation [42–44], and organelle positioning [45–47] that are likely dependent on the ability to assemble into a highly organized orthogonal grid [8]. We have recently shown that the microtubule lattices of *mdx* skeletal muscle expressing micro-dystrophins are not restored to wildtype [16]. Here we have established roles for dystrophin R4-15 and R20-23, cytoplasmic actins, and α-dystrobrevin as critical for mechanical stability of the microtubule lattice. In the absence of any of these components, the microtubule lattice was susceptible to significant loss of transverse microtubules immediately following the increased mechanical challenge of eccentric contraction. Micro-dystrophins with deletion of both R4-15 and R20-23 lost virtually all transverse microtubules upon eccentric contraction.

Microtubule loss in the absence of dystrophin R4-15 or R20-24 required simultaneous muscle lengthening and force generation of eccentric contractions. While eccentric contractions are the highest force producing [48] and most damaging type of muscle contraction [49], they are physiological [50] and very often used as an endpoint measurement for therapeutic improvement in preclinical studies of DMD [23,51]. The microtubule lattice in transgenic *mdx* mice expressing truncated dystrophins was not affected by isometric contractions, which do not cause force loss in *mdx* muscle [17]. In contrast, passive lengthening of *mdx* muscle has been shown to induce mechanotransduction through the detyrosinated-tubulin microtubule lattice to stimulate

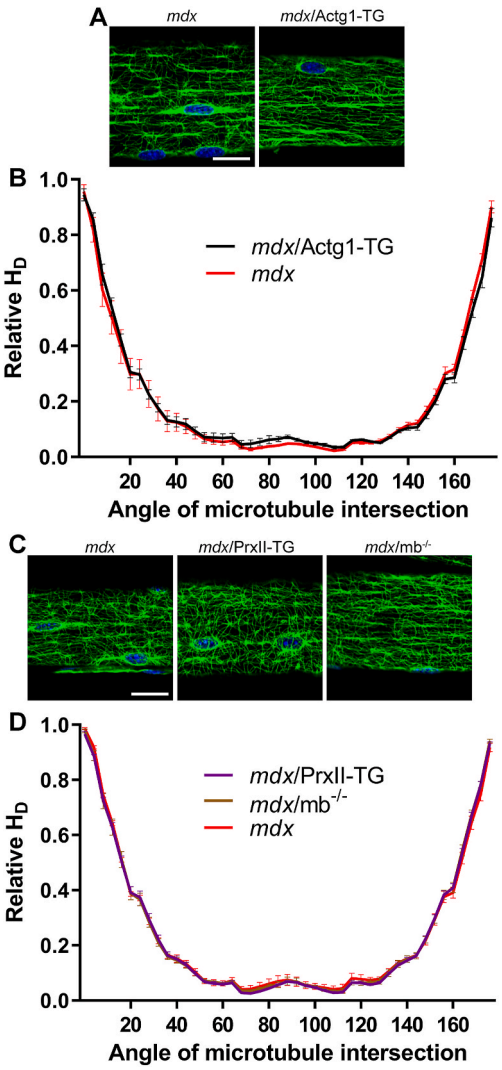

Fig. 4. Microtubules remained disorganized in *mdx*/Actg1-TG, *mdx*/PrxII-TG and *mdx*/mb$^{-/-}$. A) Both *mdx* and *mdx*/Actg1-TG had disorganized microtubule lattices. Images are representative of n ≥ 10 fibers from N = 4 *mdx*/Actg1-TG and N = 3 transgene negative *mdx* littermates. B) No significant difference in the microtubule lattice organization was detected between *mdx*/Actg1-TG and *mdx*. C) *Mdx*/PrxII-TG and *mdx*/mb$^{-/-}$ also have disorganized microtubules. Representative of n ≥ 10 fibers from N = 4 each genotype (*mdx*/PrxII-TG, *mdx*/mb$^{-/-}$ and *mdx*). Tubulin in green, nuclei in blue. Scale bar is 20 μm, 60× magnification. D) Quantification of the microtubule lattice directionality did not identify any significant differences in organization of *mdx*/PrxII-TG or *mdx*/mb$^{-/-}$ compared to *mdx*. Two-way ANOVA interaction for each genotype compared to *mdx* was not significant. Main effect of EDL was also not significant. Error bars are mean ± SEM.

heightened NOX2 ROS [12,13], although force loss does not result [19]. Here we found that passive muscle lengthening had no effect on microtubule organization in *mdx* mice expressing mini- or micro-dystrophin, which also presented with wildtype levels of detyrosinated tubulin [16]. Thus, any ROS generated by NOX2 during passive lengthening [13] was insufficient to impact microtubule organization in *mdx* mice expressing mini- or micro-dystrophin, suggesting eccentric contraction may elicit greater magnitude of ROS production through NOX2. We also analyzed the microtubule lattice after five and ten day recovery periods following eccentric contraction. Both mini- and micro-dystrophin transgenic *mdx* had deficits in transverse microtubules five days after eccentric contraction that were restored to the level of contralateral muscles by ten days. Overall, transverse microtubule loss was rapid and recovery was much slower.

Our proteomic screens identified over two thousand and three thousand proteins in the microtubule and DGC enrichments, respectively. In each of the three experimental lines (Dys$^{\Delta H2\text{-}R15}$-*mdx*, Dys$^{\Delta MTB}$-*mdx*, Dys$^{\Delta R4\text{-}23/\Delta CT}$-*mdx*) compared to Dys$^{\Delta 71\text{-}78}$-*mdx* there were over four hundred proteins of significantly different abundance in the microtubule enrichment and over five hundred proteins of significant abundance difference in the WGA enrichment. As expected, there was minimal overlap between mouse lines in a manner that would represent a dystrophin domain specific interaction. Both Dys$^{\Delta H2\text{-}R15}$-*mdx* and Dys$^{\Delta R4\text{-}23/\Delta CT}$-*mdx* (a possible R4-15 mechanism) as well as Dys$^{\Delta MTB}$-*mdx* and Dys$^{\Delta R4\text{-}23/\Delta CT}$-*mdx* (a possible R20-23 mechanism) had less than 20 proteins with similar abundance alterations as compared to Dys$^{\Delta 71\text{-}78}$-*mdx*. Of the twelve proteins selected as possible links between microtubules and a single, or both, dystrophin domains, none preserved the correlation between abundance of the selected protein and the presence/absence of dystrophin domains when expanded to additional mouse lines. Utilizing this proteomic dataset, we did not identify any protein changes that could explain a pre-existing susceptibility to eccentric contractions in *mdx* mice expressing truncated dystrophins. While altered tubb6 expression impacts microtubule organization during muscle differentiation and regeneration in *mdx* [14], we show that tubb6 levels were not different from wildtype in the transgenic mini- and micro-dystrophin *mdx* lines, nor did they change after eccentric contraction. However, our data showing rapid eccentric contraction-induced loss of transverse microtubules in *mdx* muscle expressing mini- or micro-dystrophin was consistent with a mechanism involving rapid microtubule depolymerization. Also consistent with depolymerization, we measured a decrease in detyrosinated α-tubulin in Dys$^{\Delta R2\text{-}15/\Delta R18\text{-}23/\Delta CT}$-*mdx* muscle challenged by eccentric contraction compared to the unchallenged contralateral muscle. The carboxypeptidase that removes the C-terminal tyrosine from α-tubulin to create the detyrosinated modification is preferentially active on polymerized tubulin [52], while the tubulin tyrosine ligase that reverses the detyrosination has a strong preference for free tubulin dimers [53]. Freshly depolymerized, detyrosinated tubulin is known to be quickly tyrosinated allowing the free tubulin pool to maintain a very low level of detyrosinated tubulin [39]. Therefore, the decrease in detyrosinated α-tubulin that we measured seems most likely to be simply reflecting depolymerization of transverse microtubules induced by eccentric contraction.

Eccentric contractions in *mdx* muscle leads to increased production of ROS in the form of hydrogen peroxide that has been implicated in rapid loss of contractile force [12,28]. We demonstrated here that a single dose of *N*-acetylcysteine administered to *mdx* mice expressing a mini- or micro-dystrophin prior to the *in vivo* eccentric contraction protocol was sufficient to completely protect against loss of transverse microtubules. *N*-acetylcysteine is a non-specific antioxidant [54] that has been shown to have a protective effect against force loss during *mdx* eccentric contractions [19,28,55] as well as effectively reduce ROS production in *mdx* skeletal muscle [55]. Due to its non-specific nature, NAC potentially diminishes ROS from multiple sources. Here we explored the contribution of ROS derived from NOX2 by dosing micro-dystrophin Dys$^{\Delta R4\text{-}23/\Delta CT}$-*mdx* mice with GSK2795039. GSK2795039 is a NOX2 inhibitor that is as effective as the NOX2 null (gp91$^{phox-/-}$) mouse in preventing ROS production in an *in vivo* model of inflammation [40]. Employing the same dosage as used previously [40], we measured only partial protection of transverse microtubules from eccentric contraction in GSK2795039 treated Dys$^{\Delta R4\text{-}23/\Delta CT}$-*mdx* mice. While these data support that NOX2-generated ROS contributes to eccentric contraction-induced transverse microtubule loss, it is not the only source. Although genetic ablation of nNOS has been shown to disrupt microtubule organization in skeletal muscle [20], our experiments demonstrate that eccentric contraction-induced similar losses of transverse microtubules in both Dys$^{\Delta R2\text{-}15/\Delta R18\text{-}23/\Delta CT}$-*mdx,* which localizes nNOS to the sarcolemma, and in Dys$^{\Delta R4\text{-}23/\Delta CT}$-*mdx,* which lacks dystrophin R16-17 necessary for sarcolemmal localization of nNOS [25,56]. As for other sources of ROS, xanthine oxidase (XO), a producer of

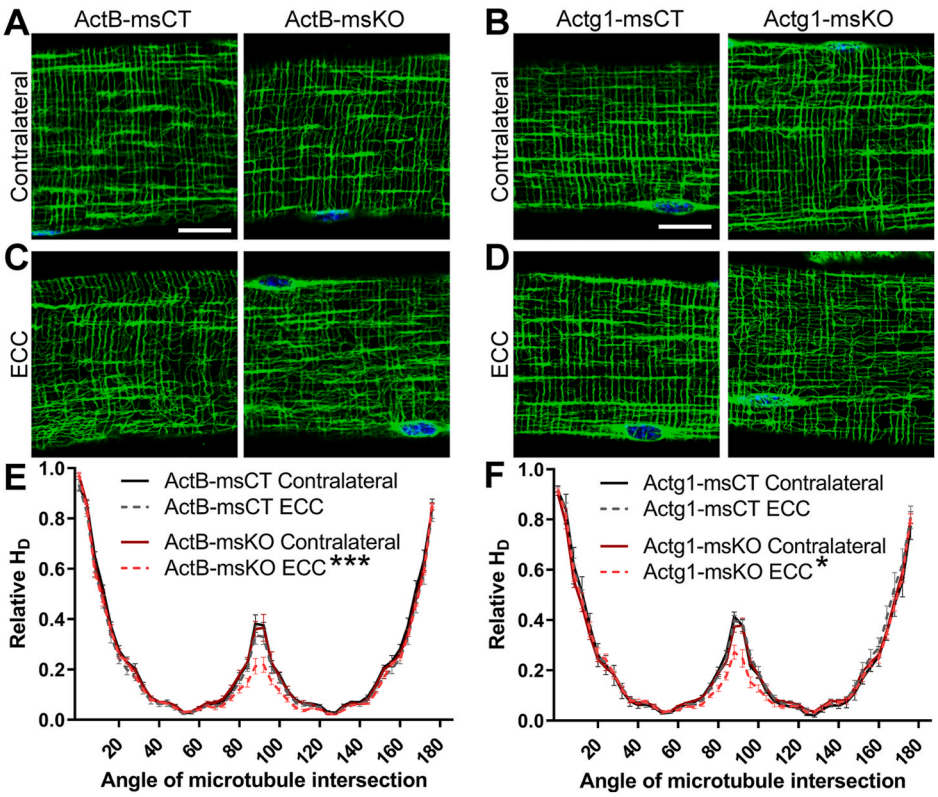

Fig. 5. Loss of cytoplasmic actin resulted in transverse microtubule loss upon eccentric contraction. A) ActB-msKO basal microtubule organization was not different than ActB-msCT. B) Actg1-msKO and Actg1-msCT had indistinguishable basal microtubule organization. C) When exposed to eccentric contraction ActB-msKO muscle lost transverse microtubules while ActB-msCT was not affected. D) Actg1-msKO muscle had notable transverse microtubule loss after eccentric contraction while Actg1-msCT did not. E) TeDT quantification of microtubule organization showed significant transverse microtubule loss in ActB-msKO following eccentric contraction, while ActB-msCT was unaffected. The loss of β-cytoplasmic actin in unchallenged muscle also did not affect the microtubule lattice. A significant ANOVA interaction was found for ActB-msKO contralateral vs ActB-msKO ECC ($p < 0.0001$). Bonferroni multiple comparison tests revealed significant (***$p < 0.001$) differences between contralateral and ECC at 84–96°. F) Eccentric contraction in Actg1-msKO muscle resulted in a significant loss of transverse microtubules. The Actg1-msCT microtubule lattice was not affected by eccentric contraction. The loss of γ-cytoplasmic actin also did not cause microtubule lattice alterations in contralateral muscle. A significant ANOVA interaction was found for Actg1-msKO contralateral vs Actg1-msKO ECC ($p < 0.0001$). Bonferroni multiple comparison tests revealed significant (*$p < 0.05$) differences between contralateral and ECC at 80°, 88–96° (84° $p = 0.053$). Two-way repeated measures ANOVA was used to compare contralateral to ECC within a genotype, while two-way ANOVA was used to compared contralateral control versus contralateral knockout. In analyses where the interaction was not significant, the main effect of EDL was not significant for both CT vs KO comparisons, and was $p = 0.002$ for Actg1-msCT contralateral vs ECC, and $p = 0.0001$ for ActB-msCT contralateral vs ECC. Images are representative of $n \geq 10$ fibers from $N = 4$ ActB-msCT, $N = 5$ ActB-msKO, $N = 3$ Actg1-msCT, and $N = 5$ Actg1-msKO. Nuclei are in blue, tubulin in green. Scale bar is 20 μm, 60× magnification. Error bars are mean ± SEM.

hydrogen peroxide and superoxide [57], has elevated activity in *mdx* skeletal muscle and inhibition with oxypurinol results in partial protection from *in vitro* eccentric contraction induced force loss [58]. NOX4, a constitutively active NOX is found at both the sarcolemma and sarcoplasmic reticulum [59]. NOX4 derived ROS has been shown to result in S-Nitrosylation of the ryanodine receptor (RyR) with pharmacologic inhibition of NOX4 in *mdx* muscle reducing RyR1 calcium leak [60]. Mitochondrial ROS, specifically from monoamine oxidase, is increased in *mdx* skeletal muscle driving tropomyosin oxidation [61], which could impact muscle contraction. XO, NOX4, and mitochondrial ROS have all been implicated in *mdx* pathology and have likely roles in muscle contraction or are located at the sarcolemma membrane and therefore could impact eccentric contraction induced transverse microtubule loss.

NOX2 and microtubule disorganization are both early pathological alterations in *mdx* and occur along a similar timeline with NOX2 increased by 19 days of age [62] and microtubule disorganization by 24 days [6]. Because genetic ablation of the p47 scaffold subunit of NOX2 in *mdx* mice results in decreased intracellular ROS [63], partial protection from eccentric contraction-induced force loss [28], and improved microtubule organization [15], we analyzed microtubule organization in three additional *mdx* models that alter ROS and exhibit partial protection from eccentric contraction-induced force loss. However, the microtubule lattice in *mdx*/Actg1-TG, *mdx*/PrxII-TG and *mdx*/mb$^{-/-}$ muscles were all as disorganized as in *mdx*. These data demonstrate that not all *mdx* lines with ROS modulations improve the basal organization of dystrophin deficient microtubules.

Given many examples of functional interaction between actin and microtubules [64], we explored the contribution of cytoplasmic actins to microtubule organization in mature skeletal muscle. We observed that skeletal muscle lacking either β-cytoplasmic or γ-cytoplasmic actin presented with wildtype microtubule lattice organization but displayed significant loss of transverse microtubules after eccentric contraction. Considering that knock out of cytoplasmic actins yields the same phenotype as *mdx* transgenic mice expressing dystrophins lacking R4-15 or R20-24, such results suggest that dystrophin mediates interaction between the actin and microtubule cytoskeletons in skeletal muscle. We observed the same phenotype in *mdx* mice expressing dystrophin with the L172H missense mutation in ABD1 that is associated with BMD. While it remains possible that L172H disrupts the actin binding function of dystrophin *in vivo*, the mutation had no significant effect on the affinity of dystrophin for actin *in vitro* [65]. L172H-*mdx* muscle also presents with reduced dystrophin levels [26]. Alternatively, ABD1 also binds directly to keratin-19 [66] while in other instances a calponin

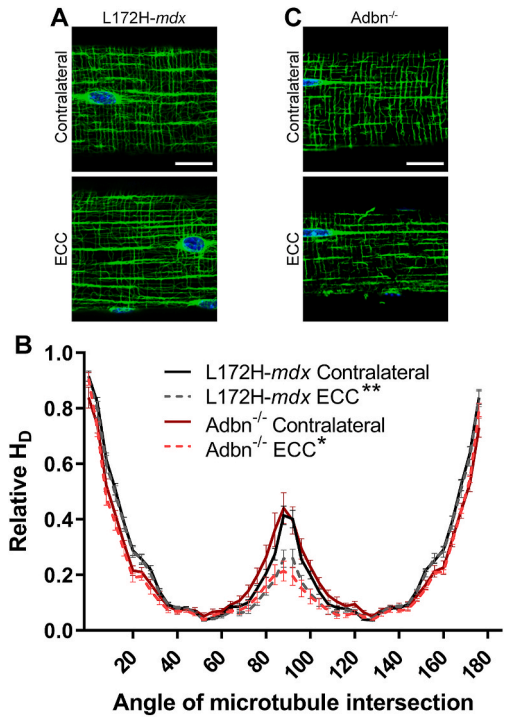

Fig. 6. ABD1 mutant L172H-*mdx* and Adbn$^{-/-}$ also had mechanically unstable microtubules. A) Expression of L172H dystrophin in *mdx* mice fully organized the microtubules in unchallenged muscle, but loss of transverse microtubules was seen following eccentric contraction. B) Quantification of the microtubule lattice revealed a significant decrease in transverse microtubules in L172H-*mdx* and Adbn$^{-/-}$ muscle after eccentric contraction. C) Adbn$^{-/-}$ contralateral muscle had well organized microtubule lattices while loss of transverse microtubules was evident upon eccentric contraction. Images are representative of n $\geq$ 10 fibers from N = 7 L172H-*mdx* and N = 5 Adbn$^{-/-}$ mice. Nuclei are in blue, tubulin in green. Scale bar is 20 μm, 60× magnification. Two-way repeated measures ANOVA within each genotype revealed a significant interaction ($p < 0.0001$) for both genotypes. Bonferroni multiple comparison tests were significant (**$p < 0.01$) at 84–96° for L172H-*mdx* and (*$p < 0.05$) at 80–100° for Adbn$^{-/-}$. Error bars are mean ± SEM.

homology (CH) domain, such as those that comprise ABD1 [67], has been shown to pair with a CH domain in another molecule to form a microtubule binding site [68]. Thus, it is possible that the L172H mutation disrupts interaction with keratin-19 or a yet-to-be identified protein containing a CH domain. Finally, we show that the microtubule lattice is rendered mechanically unstable by genetic ablation of the DGC protein α-dystrobrevin. Adbn$^{-/-}$ muscle expresses wildtype dystrophin levels but shows reduced stability of the dystrophin-DGC connection [69].

Our data demonstrate that dystrophin R4-15, dystrophin R20-23, cytoplasmic actins, and α-dystrobrevin contribute to mechanically stabilizing transverse microtubules when the muscle is under heightened physical challenge, such as eccentric contraction. While the immediate loss of transverse microtubules after eccentric contraction can be explained by rapid microtubule depolymerization, the slow (5–10 day) recovery of transverse microtubules rules out a mechanism involving simple microtubule depolymerization and re-polymerization dynamics. Based on the 3–5 μm/min rate of microtubule growth in flexor digitorum brevis fibers via intravital imaging [70], a 50 μm muscle fiber would be expected to recover transverse microtubules within 30–60 min. The lack of rapid transverse microtubule recovery is indicative of a microtubule polymerization or stabilization roadblock that requires days for muscle to overcome. Moreover, our experiments with *N*-acetylcysteine and NOX2 suggest that a non-, or very slowly reversible oxidation of one or more components of the microtubule cytoskeleton may drive the rapid loss and slow recovery of transverse microtubules. There is precedent for oxidation of tubulin and microtubule associated proteins as well as ROS-mediated inhibition of tubulin polymerization [71]. While eccentric contraction-induced ROS disrupts transverse microtubules from organized lattices, we did not see restoration of microtubules in the *mdx*/Actg1-TG, *mdx*/PrxII-TG and *mdx*/mb$^{-/-}$ lines.

In summary, we have identified three states of microtubule pathology in skeletal muscle: 1) wildtype organized microtubule lattices that are mechanically unstable such as in *mdx* muscle expressing mini-dystrophin, cytoplasmic actin knockout, or α-dystrobrevin null; 2) partially organized microtubule lattices that are mechanically unstable such as *mdx* with micro-dystrophin transgenes; 3) microtubule lattices that are completely disorganized such as in *mdx* or β-sarcoglycan null muscle [6,7,9]. ROS sources such as NOX2, but not nNOS, are involved in transverse microtubule loss from organized but mechanically unstable microtubule lattices. Future studies will investigate additional sources and targets of ROS that mediate microtubule susceptibility to eccentric contraction.

Declaration of competing interest

The authors do not have any conflicts of interest to declare.

Acknowledgements

The TMT proteomic screen was performed at the University of Minnesota Center for Mass Spectrometry and Proteomics. This work was supported by the National Institute of Arthritis and Musculoskeletal and Skin Diseases [R01 AR042423 to J.M.E. and F13 AR073629 to D.M.N.]. The funding source had no role in conduct of research or article preparation.

Appendix A. Supplementary data

Supplementary data to this article can be found online at https://doi.org/10.1016/j.redox.2020.101730.

References

[1] D.J. Blake, A. Weir, S.E. Newey, K.E. Davies, Function and genetics of dystrophin and dystrophin-related proteins in muscle, Physiol. Rev. 82 (2) (2002) 291–329.
[2] F. Rahimov, L.M. Kunkel, Cellular and molecular mechanisms underlying muscular dystrophy, J. Cell Biol. 201 (4) (2013 May) 499–510.
[3] B. Mokri, A.G. Engel, Duchenne dystrophy: electron microscopic findings pointing to a basic or early abnormality in the plasma membrane of the muscle fiber, Neurology 25 (12) (1975 Dec) 1111–1120.
[4] E.P. Hoffman, R.H. Brown, L.M. Kunkel, Dystrophin: the protein product of the duchenne muscular dystrophy locus, Cell 51 (6) (1987 Dec 24) 919–928.
[5] M. Koenig, A.H. Beggs, M. Moyer, S. Scherpf, K. Heindrich, T. Bettecken, et al., The molecular basis for Duchenne versus Becker muscular dystrophy: correlation of severity with type of deletion, Am. J. Hum. Genet. 45 (4) (1989) 498–506.
[6] K.W. Prins, J.L. Humston, A. Mehta, V. Tate, E. Ralston, J.M. Ervasti, Dystrophin is a microtubule-associated protein, J. Cell Biol. 186 (3) (2009) 363–369.
[7] J.M. Percival, P. Gregorevic, G.L. Odom, G.B. Banks, J.S. Chamberlain, S. C. Froehner, rAAV6-Microdystrophin rescues aberrant golgi complex organization in mdx skeletal muscles, Traffic 8 (10) (2007 Oct) 1424–1439.
[8] E. Ralston, T. Ploug, J. Kalhovde, T. Lomo, Golgi complex, endoplasmic reticulum exit sites, and microtubules in skeletal muscle fibers are organized by patterned activity, J. Neurosci. 21 (3) (2001) 875–883.
[9] J.J. Belanto, J.T. Olthoff, T.L. Mader, C.M. Chamberlain, D.M. Nelson, P. M. McCourt, et al., Independent variability of microtubule perturbations associated with dystrophinopathy, Hum. Mol. Genet. 25 (22) (2016 Sep 16) 4951–4961.
[10] M. Pearce, D.J. Blake, J.M. Tinsley, B.C. Byth, L. Campbell, A.P. Monaco, et al., The utrophin and dystrophin genes share similarities in genomic structure, Hum. Mol. Genet. 2 (11) (1993 Nov) 1765–1772.
[11] J.J. Belanto, T.L. Mader, M.D. Eckhoff, D.M. Strandjord, G.B. Banks, M.K. Gardner, et al., Microtubule binding distinguishes dystrophin from utrophin, Proc. Natl. Acad. Sci. Unit. States Am. 111 (15) (2014 Apr 15) 5723–5728.
[12] R.J. Khairallah, G. Shi, F. Sbrana, B.L. Prosser, C. Borroto, M.J. Mazaitis, et al., Microtubules underlie dysfunction in duchenne muscular dystrophy, Sci. Signal. 5 (236) (2012) ra56.
[13] J.P. Kerr, P. Robison, G. Shi, A.I. Bogush, A.M. Kempema, J.K. Hexum, et al., Detyrosinated microtubules modulate mechanotransduction in heart and skeletal muscle, Nat. Commun. 6 (1) (2015 Dec 8) 8526.

[14] D. Randazzo, U. Khalique, J.J. Belanto, A. Kenea, D.M. Talsness, J.T. Olthoff, et al., Persistent upregulation of the β-tubulin tubb6, linked to muscle regeneration, is a source of microtubule disorganization in dystrophic muscle, Hum. Mol. Genet. 28 (7) (2019) 1117–1135.
[15] J.A. Loehr, S. Wang, T.R. Cully, R. Pal, I.V. Larina, K.V. Larin, et al., NADPH oxidase mediates microtubule alterations and diaphragm dysfunction in dystrophic mice, Elife (e31732) (2018 Jan 30) 7.
[16] D.M. Nelson, A. Lindsay, L.M. Judge, D. Duan, J.S. Chamberlain, D.A. Lowe, et al., Variable rescue of microtubule and physiological phenotypes in mdx muscle expressing different miniaturized dystrophins, Hum. Mol. Genet. 27 (12) (2018) 2090–2100.
[17] P. Moens, P.H. Baatsen, G. Maréchal, Increased susceptibility of EDL muscles from mdx mice to damage induced by contractions with stretch, J. Muscle Res. Cell Motil. 14 (4) (1993 Aug) 446–451.
[18] B.J. Petrof, J.B. Shrager, H.H. Stedman, a M. Kelly, H.L. Sweeney, Dystrophin protects the sarcolemma from stresses developed during muscle contraction, Proc. Natl. Acad. Sci. U. S. A. 90 (8) (1993) 3710–3714.
[19] A. Lindsay, C.W. Baumann, R.T. Rebbeck, S.L. Yuen, W.M. Southern, J.S. Hodges, et al., Mechanical factors tune the sensitivity of mdx muscle to eccentric strength loss and its protection by antioxidant and calcium modulators, Skeletal Muscle 10 (1) (2020 Dec 1) 3.
[20] Y. Moon, J.E. Balke, D. Madorma, M.P. Siegel, G. Knowels, P. Brouckaert, et al., Nitric oxide regulates skeletal muscle fatigue, fiber fype, microtubule organization, and mitochondrial ATP synthesis efficiency through cGMP-dependent mechanisms, Antioxidants Redox Signal. 26 (17) (2017 Jun 10) 966–985.
[21] M.J. Blankinship, P. Gregorevic, J.S. Chamberlain, Gene therapy strategies for Duchenne muscular dystrophy utilizing recombinant adeno-associated virus vectors, Mol. Ther. 13 (2) (2006) 241–249.
[22] D. Duan, Systemic AAV micro-dystrophin gene therapy for Duchenne muscular dystrophy, Mol. Ther. 26 (10) (2018 Oct 3) 2337–2356.
[23] J.N. Ramos, K. Hollinger, N.E. Bengtsson, J.M. Allen, S.D. Hauschka, J. S. Chamberlain, Development of novel micro-dystrophins with enhanced functionality, Mol. Ther. 27 (3) (2019 Jan 25) 623–635.
[24] S. Li, E. Kimura, R. Ng, B.M. Fall, L. Meuse, M. Reyes, et al., A highly functional mini-dystrophin/GFP fusion gene for cell and gene therapy studies of Duchenne muscular dystrophy, Hum. Mol. Genet. 15 (10) (2006) 1610–1622.
[25] Y. Lai, G.D. Thomas, Y. Yue, H.T. Yang, D. Li, C. Long, et al., Dystrophins carrying spectrin-like repeats 16 and 17 anchor nNOS to the sarcolemma and enhance exercise performance in a mouse model of muscular dystrophy, J. Clin. Invest. 119 (3) (2009) 624–635.
[26] J.L. McCourt, D.M. Talsness, A. Lindsay, R.W. Arpke, P.D. Chatterton, D.M. Nelson, et al., Mouse models of two missense mutations in actin-binding domain 1 of dystrophin associated with duchenne or becker muscular dystrophy, Hum. Mol. Genet. 27 (3) (2018) 451–462.
[27] S.A. Hamed, A.J. Sutherland-Smith, J.R.M. Gorospe, J. Kendrick-Jones, E. P. Hoffman, DNA sequence analysis for structure/function and mutation studies in Becker muscular dystrophy, Clin. Genet. 68 (1) (2005 May 4) 69–79.
[28] J.T. Olthoff, A. Lindsay, R. Abo-Zahrah, K.A. Baltgalvis, X. Patrinostro, J.J. Belanto, et al., Loss of peroxiredoxin-2 exacerbates eccentric contraction-induced force loss in dystrophin-deficient muscle, Nat. Commun. 9 (1) (2018 Dec 30) 5104.
[29] D. Li, Y. Yue, Y. Lai, C.H. Hakim, D. Duan, Nitrosative stress elicited by nNOSμ delocalization inhibits muscle force in dystrophin-null mice, J. Pathol. 223 (1) (2011 Jan) 88–98.
[30] L.M. Judge, M. Haraguchiln, J.S. Chamberlain, Dissecting the signaling and mechanical functions of the dystrophin-glycoprotein complex, J. Cell Sci. 119 (Pt 8) (2006) 1537–1546.
[31] K.J. Sonnemann, D.P. Fitzsimons, J.R. Patel, Y. Liu, M.F. Schneider, R.L. Moss, et al., Cytoplasmic γ-actin is not required for skeletal muscle development but its absence leads to a progressive myopathy, Dev. Cell 11 (3) (2006 Sep) 387–397.
[32] K.W. Prins, J.A. Call, D.A. Lowe, J.M. Ervasti, Quadriceps myopathy caused by skeletal muscle-specific ablation of βcyto-actin, J. Cell Sci. 124 (6) (2011 Mar 15) 951–957.
[33] K.A. Baltgalvis, M.A. Jaeger, D.P. Fitzsimons, S.A. Thayer, D.A. Lowe, J.M. Ervasti, Transgenic overexpression of γ-cytoplasmic actin protects against eccentric contraction-induced force loss in mdx mice, Skeletal Muscle 1 (1) (2011) 32.
[34] R.M. Grady, R.W. Grange, K.S. Lau, M.M. Maimone, M.C. Nichol, J.T. Stull, et al., Role for α-dystrobrevin in the pathogenesis of dystrophin-dependent muscular dystrophies, Nat. Cell Biol. 1 (4) (1999 Jul 8) 215–220.
[35] J.A. Call, M.D. Eckhoff, K.A. Baltgalvis, G.L. Warren, D.A. Lowe, Adaptive strength gains in dystrophic muscle exposed to repeated bouts of eccentric contraction, J. Appl. Physiol. 111 (6) (2011 Dec) 1768–1777.
[36] W. Liu, E. Ralston, A new directionality tool for assessing microtubule pattern alterations, Cytoskeleton 71 (4) (2014) 230–240.
[37] G.G. Gundersen, M.H. Kalnoski, J.C. Bulinski, Distinct populations of microtubules: tyrosinated and nontyrosinated alpha tubulin are distributed differently in vivo, Cell 38 (3) (1984 Oct) 779–789.
[38] G.G. Gundersen, S. Khawaja, J.C. Bulinski, Generation of a stable, posttranslationally modified microtubule array is an early event in myogenic differentiation, J. Cell Biol. 109 (5) (1989 Nov 1) 2275–2288.
[39] G.G. Gundersen, S. Khawaja, J.C. Bulinski, Postpolymerization detyrosination of alpha-tubulin: a mechanism for subcellular differentiation of microtubules, J. Cell Biol. 105 (1) (1987) 251–264.
[40] K. Hirano, W.S. Chen, A.L.W. Chueng, A.A. Dunne, T. Seredenina, A. Filippova, et al., Discovery of GSK2795039, a novel small molecule NADPH oxidase 2 inhibitor, Antioxidants Redox Signal. 23 (5) (2015 Aug 10) 358–374.
[41] I.N. Rybakova, J.R. Patel, J.M. Ervasti, The dystrophin complex forms a mechanically strong link between the sarcolemma and costameric actin, J. Cell Biol. 150 (5) (2000) 1209–1214.
[42] B. Mogessie, D. Roth, Z. Rahil, A. Straube, A novel isoform of MAP4 organises the paraxial microtubule array required for muscle cell differentiation, Elife 4 (4) (2015 Apr 21) 1–28.
[43] T. Zhang, K.J.M. Zaal, J. Sheridan, A. Mehta, G.G. Gundersen, E. Ralston, Microtubule plus-end binding protein EB1 is necessary for muscle cell differentiation, elongation and fusion, J. Cell Sci. 122 (9) (2009 May 1) 1401–1409.
[44] A. Straube, A. Merdes, EB3 regulates microtubule dynamics at the cell cortex and is required for myoblast elongation and fusion, Curr. Biol. 17 (15) (2007 Aug 7) 1318–1325.
[45] H. Elhanany-Tamir, Y.V. Yu, M. Shnayder, A. Jain, M. Welte, T. Volk, Organelle positioning in muscles requires cooperation between two KASH proteins and microtubules, J. Cell Biol. 198 (5) (2012) 833–846.
[46] B. Cadot, V. Gache, E. Vasyutina, S. Falcone, C. Birchmeier, E.R. Gomes, Nuclear movement during myotube formation is microtubule and dynein dependent and is regulated by Cdc 42, Par 6 and Par 3, EMBO Rep. 13 (8) (2012) 741–749.
[47] T. Metzger, V. Gache, M. Xu, B. Cadot, E.S. Folker, B.E. Richardson, et al., MAP and kinesin-dependent nuclear positioning is required for skeletal muscle function, Nature 484 (7392) (2012 Mar 18) 120–124.
[48] T. Hortobágyi, F.I. Katch, Eccentric and concentric torque-velocity relationships during arm flexion and extension. Influence of strength level, Eur. J. Appl. Physiol. Occup. Physiol. 60 (5) (1990) 395–401.
[49] J. Fridén, R.L. Lieber, Structural and mechanical basis of exercise-induced muscle injury, Med. Sci. Sports Exerc. 24 (5) (1992) 521–529.
[50] S. Hody, J.-L. Croisier, T. Bury, B. Rogister, P. Leprince, Eccentric muscle contractions: risks and benefits, Front. Physiol. 10 (2019 May 3) 536.
[51] S. Guiraud, B. Edwards, A. Babbs, S.E. Squire, A. Berg, L. Moir, et al., The potential of utrophin and dystrophin combination therapies for Duchenne muscular dystrophy, Hum. Mol. Genet. 28 (13) (2019 Jul 1) 2189–2200.
[52] N. Kumar, M. Flavin, Preferential action of a brain detyrosinolating carboxypeptidase on polymerized tubulin, J. Biol. Chem. 256 (14) (1981 Jul 25) 7678–7686.
[53] D.R. Webster, G.G. Gundersen, J.C. Bulinski, G.G. Borisy, Assembly and turnover of detyrosinated tubulin in vivo, J. Cell Biol. 105 (1) (1987) 265–276.
[54] Y. Samuni, S. Goldstein, O.M. Dean, M. Berk, The chemistry and biological activities of N-acetylcysteine, Biochim. Biophys. Acta 1830 (8) (2013 Aug 1) 4117–4129.
[55] N.P. Whitehead, C. Pham, O.L. Gervasio, D.G. Allen, N-Acetylcysteine ameliorates skeletal muscle pathophysiology in mdx mice, J. Physiol. 586 (7) (2008 Apr 1) 2003–2014.
[56] M.E. Adams, G.L. Odom, M.J. Kim, J.S. Chamberlain, S.C. Froehner, Syntrophin binds directly to multiple spectrin-like repeats in dystrophin and mediates binding of nNOS to repeats 16-17, Hum. Mol. Genet. 27 (17) (2018) 2978–2985.
[57] E.E. Kelley, N.K.H. Khoo, N.J. Hundley, U.Z. Malik, B.A. Freeman, M.M. Tarpey, Hydrogen peroxide is the major oxidant product of xanthine oxidase, Free Radic. Biol. Med. 48 (4) (2010 Feb 15) 493–498.
[58] A. Lindsay, P.M. McCourt, P. Karachunski, D.A. Lowe, J.M. Ervasti, Xanthine oxidase is hyper-active in Duchenne muscular dystrophy, Free Radic. Biol. Med. 129 (2018 Dec) 364–371.
[59] G.K. Sakellariou, M.J. Jackson, A. Vasilaki, Redefining the major contributors to superoxide production in contracting skeletal muscle. The role of NAD(P)H oxidases, Free Radic. Res. 48 (1) (2014 Jan) 12–29.
[60] T.R. Cully, G.G. Rodney, Nox4 – RyR1 – nox2: regulators of micro-domain signaling in skeletal muscle, Redox Biol 36 (2020 Sep 1) 101557.
[61] S. Menazza, B. Blaauw, T. Tiepolo, L. Toniolo, P. Braghetta, B. Spolaore, et al., Oxidative stress by monoamine oxidases is causally involved in myofiber damage in muscular dystrophy, Hum. Mol. Genet. 19 (21) (2010) 4207–4215.
[62] N.P. Whitehead, E.W. Yeung, S.C. Froehner, D.G. Allen, Skeletal muscle NADPH oxidase is increased and triggers stretch-induced damage in the mdx mouse. Tarnopolsky MA, PloS One 5 (12) (2010 Dec 20), e15354.
[63] R. Pal, M. Palmieri, J a Loehr, S. Li, R. Abo-Zahrah, T.O. Monroe, et al., Src-dependent impairment of autophagy by oxidative stress in a mouse model of Duchenne muscular dystrophy, Nat. Commun. 5 (1) (2014 Dec 16) 4425.
[64] M. Dogterom, G.H. Koenderink, Actin–microtubule crosstalk in cell biology, Nat. Rev. Mol. Cell Biol. 20 (1) (2019 Jan 15) 38–54.
[65] D.M. Henderson, A. Lee, J.M. Ervasti, Disease-causing missense mutations in actin binding domain 1 of dystrophin induce thermodynamic instability and protein aggregation, Proc. Natl. Acad. Sci. U. S. A. 107 (21) (2010 May 25) 9632–9637.
[66] M.R. Stone, A. O'Neill, D. Catino, R.J. Bloch, Specific interaction of the actin-binding domain of dystrophin with intermediate filaments containing keratin 19, Mol. Biol. Cell 16 (9) (2005 Sep) 4280–4293.
[67] F.L.M. Norwood, A.J. Sutherland-Smith, N.H. Keep, J. Kendrick-Jones, The structure of the N-terminal actin-binding domain of human dystrophin and how mutations in this domain may cause Duchenne or Becker muscular dystrophy, Structure 8 (5) (2000 May 1) 481–491.
[68] B. Sjöblom, J. Ylänne, K. Djinović-Carugo, Novel structural insights into F-actin-binding and novel functions of calponin homology domains, Curr. Opin. Struct. Biol. 18 (6) (2008 Dec 1) 702–708.

[69] T.M. Bunnell, M.A. Jaeger, D.P. Fitzsimons, K.W. Prins, J.M. Ervasti, Destabilization of the dystrophin-glycoprotein complex without functional deficits in α-dystrobrevin null muscle, PloS One 3 (7) (2008 Jul 2), e2604.
[70] S. Oddoux, K.J. Zaal, V. Tate, A. Kenea, S.A. Nandkeolyar, E. Reid, et al., Microtubules that form the stationary lattice of muscle fibers are dynamic and nucleated at golgi elements, J. Cell Biol. 203 (2) (2013) 205–213.
[71] C. Wilson, C. González-Billault, Regulation of cytoskeletal dynamics by redox signaling and oxidative stress: implications for neuronal development and trafficking, Front. Cell. Neurosci. 9 (SEPTEMBER) (2015 Sep 30) 381.